



Variations in Seawater $p\text{CO}_2$ Associated With Vertical Mixing During Tropical Cyclone Season in the Northwestern Subtropical Pacific Ocean

OPEN ACCESS

Young Ho Ko¹, Geun-Ha Park^{2*†}, Dongseon Kim² and Tae-Wook Kim^{1,3*†}

Edited by:

Johan Schijf,
University of Maryland Center for
Environmental Science (UMCES),
United States

Reviewed by:

Wei-dong Zhai,
Shandong University, China
Gilles Reverdin,
Centre National de la Recherche
Scientifique (CNRS), France
Rik Wanninkhof,
National Oceanic and Atmospheric
Administration (NOAA), United States

*Correspondence:

Geun-Ha Park
gpark@kiost.ac.kr
Tae-Wook Kim
kimtwk@korea.ac.kr

† These authors have contributed
equally to this work

Specialty section:

This article was submitted to
Marine Biogeochemistry,
a section of the journal
Frontiers in Marine Science

Received: 11 March 2021

Accepted: 15 June 2021

Published: 06 July 2021

Citation:

Ko Y, Park G-H, Kim D and
Kim T-W (2021) Variations
in Seawater $p\text{CO}_2$ Associated With
Vertical Mixing During Tropical
Cyclone Season in the Northwestern
Subtropical Pacific Ocean.
Front. Mar. Sci. 8:679314.
doi: 10.3389/fmars.2021.679314

¹ OJ Eong Resilience Institute, Korea University, Seoul, South Korea, ² Marine Environmental Research Center, Korea Institute of Ocean Science and Technology, Busan, South Korea, ³ Division of Environmental Science and Ecological Engineering, Korea University, Seoul, South Korea

This study examines interannual variations in the seawater CO_2 partial pressure ($p\text{CO}_2$) for months (August–October) with frequent tropical cyclone (TC) events in the northwestern subtropical Pacific Ocean (22°N – 28°N , 135°E – 145°E) between 2007 and 2017. The temperature-normalized $p\text{CO}_2$ averaged over August–October showed a year-to-year variation ranging from 346 to 359 μatm over the 11 study years, which appeared to be related to the variation in vertical mixing that likely results from the TC activity in these months. Sea surface temperature and wind data consistently supported the association between mixing and TC intensity. Nonetheless, the $p\text{CO}_2$ reduction caused by negative sea-surface temperature anomalies found over the TC season (July–October) shifted the study area from a CO_2 source to a CO_2 sink over these months. In the south (17°N – 22°N) of the study area, mixing-driven variations in $p\text{CO}_2$ were smaller during the same months, which appeared to be caused by the relatively deeper mixed layer depth and the more homogenous profile of CO_2 in this tropical region. These results suggest that more extensive $p\text{CO}_2$ measurements are required to fully resolve the effect of TCs on the carbonate system from the regional- to the basin-scale in the western Pacific Ocean, where TC intensity is expected to increase in the future.

Keywords: tropical cyclone, seawater CO_2 partial pressure, subtropical Pacific Ocean, vertical mixing, sea surface temperature

INTRODUCTION

The measurement of surface seawater CO_2 partial pressure ($p\text{CO}_2$) allows the estimation of the oceanic uptake of anthropogenic CO_2 . Although global air–sea CO_2 flux estimates are available using ship-based $p\text{CO}_2$ observations ($p\text{CO}_2^{\text{obs}}$) conducted over the last three decades, uncertainties remain due to spatiotemporal biases in oceanic $p\text{CO}_2^{\text{obs}}$ data and the insufficient understanding of seasonal and interannual $p\text{CO}_2$ variability (Takahashi et al., 2009; Wanninkhof et al., 2013; Landschützer et al., 2016). Ocean carbonate variables affecting surface $p\text{CO}_2$ change according to

seasonal variations caused by physical and biogeochemical processes (Takahashi et al., 1993, 2002). In the subtropics, $p\text{CO}_2$ is primarily regulated by seasonal variations in temperature, whereas at higher latitudes, its oscillation is typically dominated by biological processes (e.g., photosynthetic CO_2 fixation and the remineralization of organic carbon). Additionally, the accurate estimation of ocean CO_2 uptake can be hampered by various interannual climate variabilities and their effects on seasonal cycles of ocean carbonate variables (Lenton et al., 2012; Sutton et al., 2017). The reduction of the buffering capacity due to the accumulation of anthropogenic CO_2 can even amplify seasonal variations of surface $p\text{CO}_2$ at the decadal timescale (Fassbender et al., 2018; Landschützer et al., 2018).

One important question regarding seasonal variations in surface $p\text{CO}_2$ and CO_2 fluxes is how episodic events change surface carbonate parameters (Chen et al., 2007; Mahadevan et al., 2011). For example, during and after the passage of a tropical cyclone (TC), the entrainment of CO_2 -rich water and the drop in temperature increase and decrease surface $p\text{CO}_2$, respectively (Bates et al., 1998; Wanninkhof et al., 2007; Nemoto et al., 2009; Huang and Imberger, 2010; Wada et al., 2014; Cheng et al., 2015). This compensatory effect is well-documented; however, regional differences in the physical and chemical properties of subsurface water result in large variability in the surface $p\text{CO}_2$ in response to TC passage (Mahadevan et al., 2011; Lévy et al., 2012; Ye et al., 2020). Phytoplankton CO_2 fixation, which is fueled by the supply of subsurface nutrients, is also highly variable in space and time (Lin, 2012; Ye et al., 2013; Wu et al., 2020; Chai et al., 2021; Zhang et al., 2021). Furthermore, the magnitude and direction of air-sea CO_2 flux during and after TC passage strongly depend on pre-storm $p\text{CO}_2$ conditions and the intensities of individual TCs (Lévy et al., 2012). For example, when a TC passes over a region that is oversaturated with atmospheric CO_2 in the summer, instantaneous wind-speed enhancement facilitates CO_2 out-gassing (Bates et al., 1998; Nemoto et al., 2009; Huang and Imberger, 2010). In contrast, the opposite is true in areas with CO_2 undersaturation. This site-specific response indicates that TC-driven $p\text{CO}_2$ changes observed at spatially limited stations (e.g., in the Sargasso Sea) cannot be extrapolated over regional and global scales (Lévy et al., 2012). Therefore, the characterization of such TC-induced changes over broad oceanic regions is required to improve the understanding and prediction of TC-derived changes in $p\text{CO}_2$ and air-sea CO_2 flux.

The western North Pacific is the most active oceanic basin with respect to TC occurrences. On average, ~ 20 TCs are formed over the western North Pacific during June–October, and ~ 13 TCs during August–September. Accordingly, the effects of TCs on surface water conditions have been examined in marginal seas (e.g., the South China Sea and the East China Sea; Nemoto et al., 2009; Ye et al., 2017) and at the Kuroshio Extension Observatory station (Bond et al., 2011; Wada et al., 2013; Chai et al., 2021) in the North Pacific. However, open waters of the northwestern subtropical Pacific Ocean (NWSP) have not been thoroughly evaluated in this regard, even though the area has some of the highest data coverage for $p\text{CO}_2^{obs}$. In this study, for the NWSP, we explored the effects of TC-driven physical

processes on interannual variations in $p\text{CO}_2$ in August–October (hereinafter “TC months”) using 11 years of $p\text{CO}_2^{obs}$ data.

DATA AND METHODS

Data Used

We used $p\text{CO}_2^{obs}$ data from the Surface Ocean CO_2 Atlas (SOCAT¹; Bakker et al., 2016). Seawater $p\text{CO}_2^{obs}$ data collected over 11 years (2007–2017) were normalized to the reference year of 2012 to remove the increasing trend caused by the oceanic uptake of anthropogenic CO_2 (Figure 1A). Using 25 years (1983–2017) of observations of $p\text{CO}_2$ and dissolved inorganic carbon (C_T) along 137°E, Ono et al. (2019) found that the rate of $p\text{CO}_2$ increase in subtropical ($>20^\circ\text{N}$) waters was $\sim 1.71 \mu\text{atm year}^{-1}$, which was close to the mean growth rate of atmospheric $p\text{CO}_2$. Furthermore, Takahashi et al. (2006) found that atmospheric and oceanic $p\text{CO}_2$ consistently increased at a similar rate in the subtropical Pacific Ocean between 1970 and 2004. Thus, we assumed that, in our study area, the oceanic $p\text{CO}_2$ increased at the same rate as the atmospheric $p\text{CO}_2$, which was $\sim 2.2 \mu\text{atm year}^{-1}$ during 2007–2017.

A study area with a size of $6^\circ \times 10^\circ$ (22°N – 28°N , 135°E – 145°E) was selected because of $p\text{CO}_2^{obs}$ data availability and the relatively shallow mixed layer depth (MLD) in this area (Figures 2A,B). The $p\text{CO}_2^{obs}$ data collected north of 28°N and south of 22°N were excluded due to the influence of the Kuroshio and North Equatorial currents, respectively. Most of the used SOCAT time-series data were collected from the south of Japan to the equatorial region along 140°E during periodic (usually monthly) surveys conducted using the Trans Future V vehicle carrier as a part of the Ship of Opportunity project². The reported CO_2 fugacity ($f\text{CO}_2$) was converted to $p\text{CO}_2$ using the formula $p\text{CO}_2 = f\text{CO}_2 \times (1.00436 - 4.669 \times 10^{-5} \times \text{SST})$, where SST is the sea-surface temperature (Takahashi et al., 2019). These converted $p\text{CO}_2$ values were 1.0–1.3 μatm greater than the $f\text{CO}_2$ values. Monthly climatology of sea surface $p\text{CO}_2$ and air-sea CO_2 flux were acquired from the gridded product of Fassbender et al. (2017) and Landschützer et al. (2020)³, respectively.

Tropical cyclone best track data recorded at 6-h intervals were obtained from the Regional Specialized Meteorological Center of the Japan Meteorological Agency (JMA⁴). Over the 11 years, the number of TCs passing over the study region during the summer ranged from 2 to 10, with an average of seven (Figure 3). Following Bell et al. (2000), the accumulated cyclone energy (ACE) index was calculated by summing the squares of the 6-hourly maximum sustained wind speed (V) obtained from the JMA best track data,

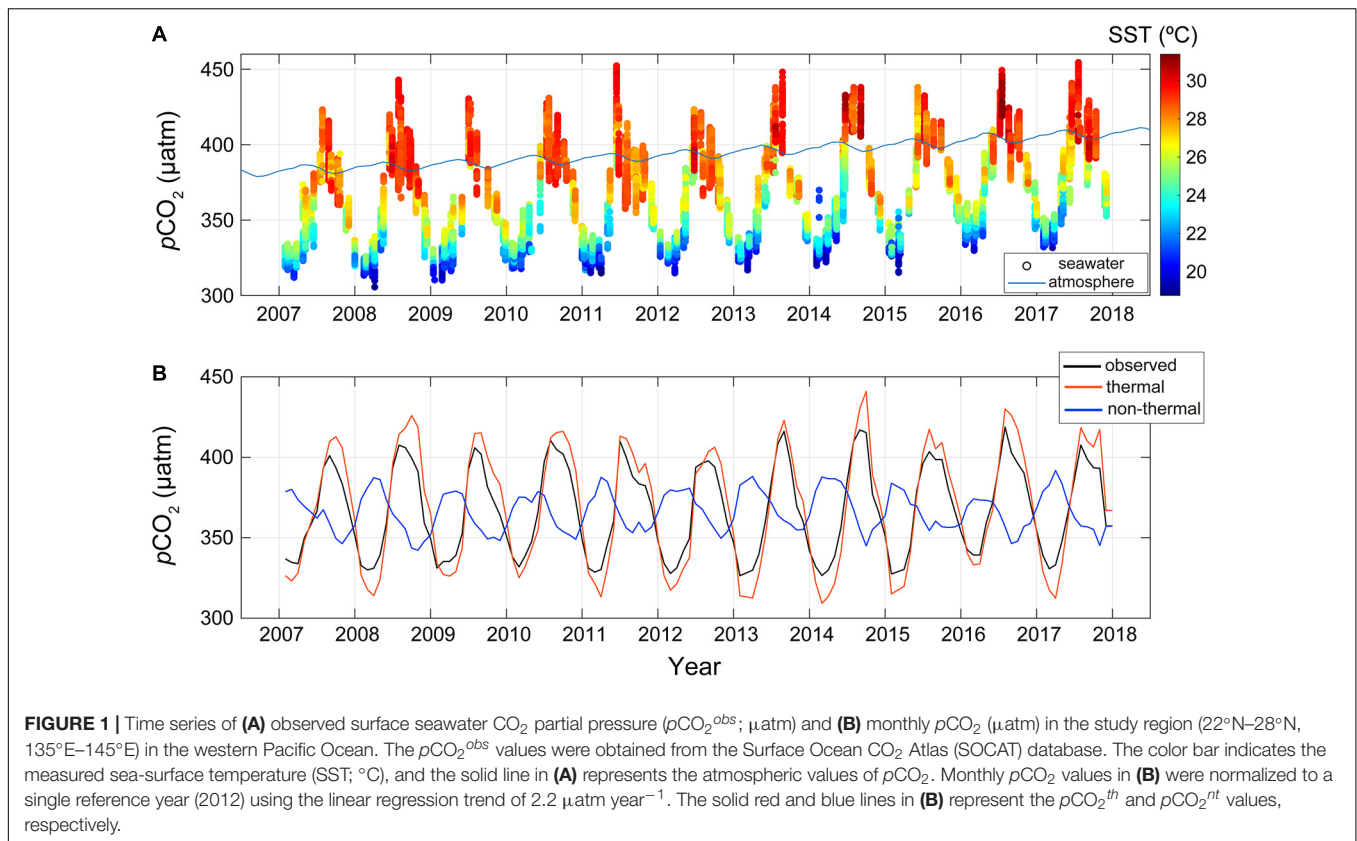
$$ACE = \sum_{i=1}^{N_{TC}} \sum_{r=1}^{N_{obs}} V^2 \quad (1)$$

¹<http://www.socat.info/>

²<http://tf5.soop.jp>

³https://www.ncei.noaa.gov/access/ocean-carbon-data-system/oceans/SPCO2_1982_present_ETH_SOM_FFN.html

⁴https://www.jma.go.jp/jma/eng/jma-center/rsmc-hp-pub-eg/RSMC_HP.htm



where the ACE index represents the overall frequency and intensity of TC events over the given period by accounting for the numbers of TC events (N_{TC}) and giving more weight to TC events with a longer duration (N_{obs}). N_{obs} indicates the number of the 6-hourly maximum sustained wind speed of each TC that passed over the study region. The ACE index can be directly associated with the magnitude of vertical mixing caused by TC events because it is proportional to the overall energy carried by the TCs.

Gridded daily SST values were obtained from the National Oceanic and Atmospheric Administration (NOAA) high-resolution SST data provided by the NOAA website⁵. The gridded daily 10-m wind speed data were obtained from the NCEP/NCAR Reanalysis 1 product (Kalnay et al., 1996⁶). MLD data were obtained from an MLD database constructed based on Argo profiles (Holte et al., 2017⁷). Vertical C_T , total alkalinity (A_T), nitrate (NO_3^-), and chlorophyll-*a* data were obtained from the Global Ocean Data Analysis Project version 2 (GLODAP v2; Olsen et al., 2016⁸). The Moderate Resolution Imaging Spectroradiometer standard chlorophyll-*a* data used in this study were obtained from the ocean color webpage operated by the National Aeronautics and Space Administration⁹. The carbonic acid dissociation constants

of Lueker et al. (2000) were used to derive a carbonate variable ($p\text{CO}_2$) from other variables (A_T and C_T). Monthly precipitation data were obtained from merged satellite and gage observations provided by the NOAA Climate Prediction Center¹⁰.

Calculation of the Thermal and Non-Thermal $p\text{CO}_2$ Components

It is well known that seasonal variations in surface $p\text{CO}_2$ can be decomposed into thermal and non-thermal upper-ocean factors. Seawater $p\text{CO}_2$ is thermodynamically dependent on temperature ($4.23\% \text{ } ^\circ\text{C}^{-1}$) (Takahashi et al., 1993, 2002). This relationship includes the effect of temperature on the solubility of CO_2 and dissociation constants of carbonic acid in seawater, which is referred to as the thermal factor. In contrast, the non-thermal factors include vertical mixing, biological processes, and air–sea CO_2 exchange; these factors influence seawater C_T , which in turn is directly related to $p\text{CO}_2$. For example, in winter, deep mixing causes $p\text{CO}_2$ to rise due to the upwelling of high- C_T waters. Then, biological C_T drawdown decreases $p\text{CO}_2$ as the MLD shoals during the subsequent phytoplankton growing seasons. In general, these thermal and non-thermal effects on $p\text{CO}_2$ cancel each other out, making it difficult to identify their individual effects on $p\text{CO}_2$ variations. To isolate the thermal effect on $p\text{CO}_2$, an empirical

⁵<https://www.esrl.noaa.gov/psd/>

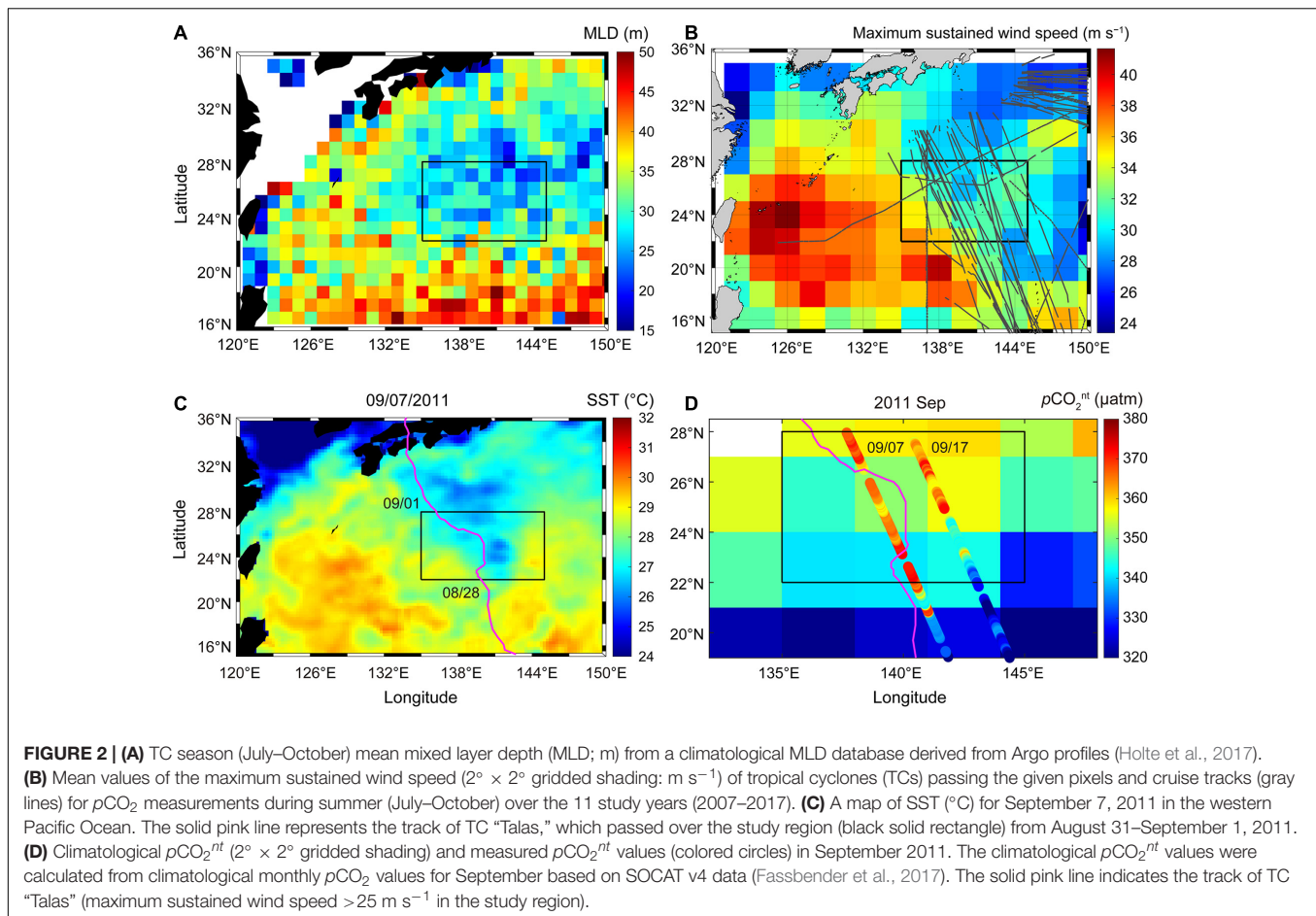
⁶<https://psl.noaa.gov/data/gridded/data.ncep.reanalysis.html>

⁷<http://www.argo.ucsd.edu>

⁸<https://www.nodc.noaa.gov/ocads/oceans/GLODAPv2/>

⁹<https://oceancolor.gsfc.nasa.gov>

¹⁰<https://psl.noaa.gov/data/gridded/data.cmap.html>



relationship ($\partial \ln p\text{CO}_2 / \partial \text{SST} = 0.0423^\circ\text{C}^{-1}$) and the following equation established by Takahashi et al. (1993, 2002) were used:

$$p\text{CO}_2^{\text{th}} = \langle p\text{CO}_2 \rangle \exp(0.0423 \times (\text{SST} - \langle \text{SST} \rangle)) \quad (2)$$

where $\langle p\text{CO}_2 \rangle$ and $\langle \text{SST} \rangle$ represent the mean $p\text{CO}_2^{\text{obs}}$ and SST values during 2007–2017, respectively. In Eq. 2, the exponential term causes $\langle p\text{CO}_2 \rangle$ to rise (drop) with increasing (decreasing) SST. The non-thermal component ($p\text{CO}_2^{nt}$), which reflects the effect of biophysical processes, was computed by normalizing the $p\text{CO}_2^{\text{obs}}$ values to $\langle \text{SST} \rangle$ as follows:

$$p\text{CO}_2^{nt} = p\text{CO}_2^{\text{obs}} \times \exp(0.0423 \times ((\text{SST}) - \langle \text{SST} \rangle)) \quad (3)$$

where the exponential term removes the SST-associated $p\text{CO}_2$ variation from the observed values. To identify the dominant factor controlling variations in $p\text{CO}_2^{nt}$, we used indicators representing mixing and biological activities, while the effect of air–sea exchange was roughly predicted using the climatological $p\text{CO}_2$ data (Landschützer et al., 2020). In general, changes in nutrient (e.g., NO_3^-) and chlorophyll-*a* concentrations can be used to examine the biological influence on $p\text{CO}_2^{nt}$. Because the thermodynamic SST effect was removed in $p\text{CO}_2^{nt}$,

SST can be used as an indicator for the effect of vertical mixing on $p\text{CO}_2^{nt}$ when the mixed layer deepens during the transition from summer to winter. To maintain the consistency of the $p\text{CO}_2^{\text{th}}$ and $p\text{CO}_2^{nt}$ values calculated from the various $p\text{CO}_2^{\text{obs}}$ datasets, including SOCAT, GLODAP, and climatological datasets, an $\langle \text{SST} \rangle$ of 26.03°C was used, which was the mean value of the reported SOCAT SST data collected over the 11 years in our study area (22°N – 28°N , 135°E – 145°E). Finally, the measured $p\text{CO}_2$ data were not normalized to a constant salinity. More details about the salinity normalization are given in section “Results and Discussion.”

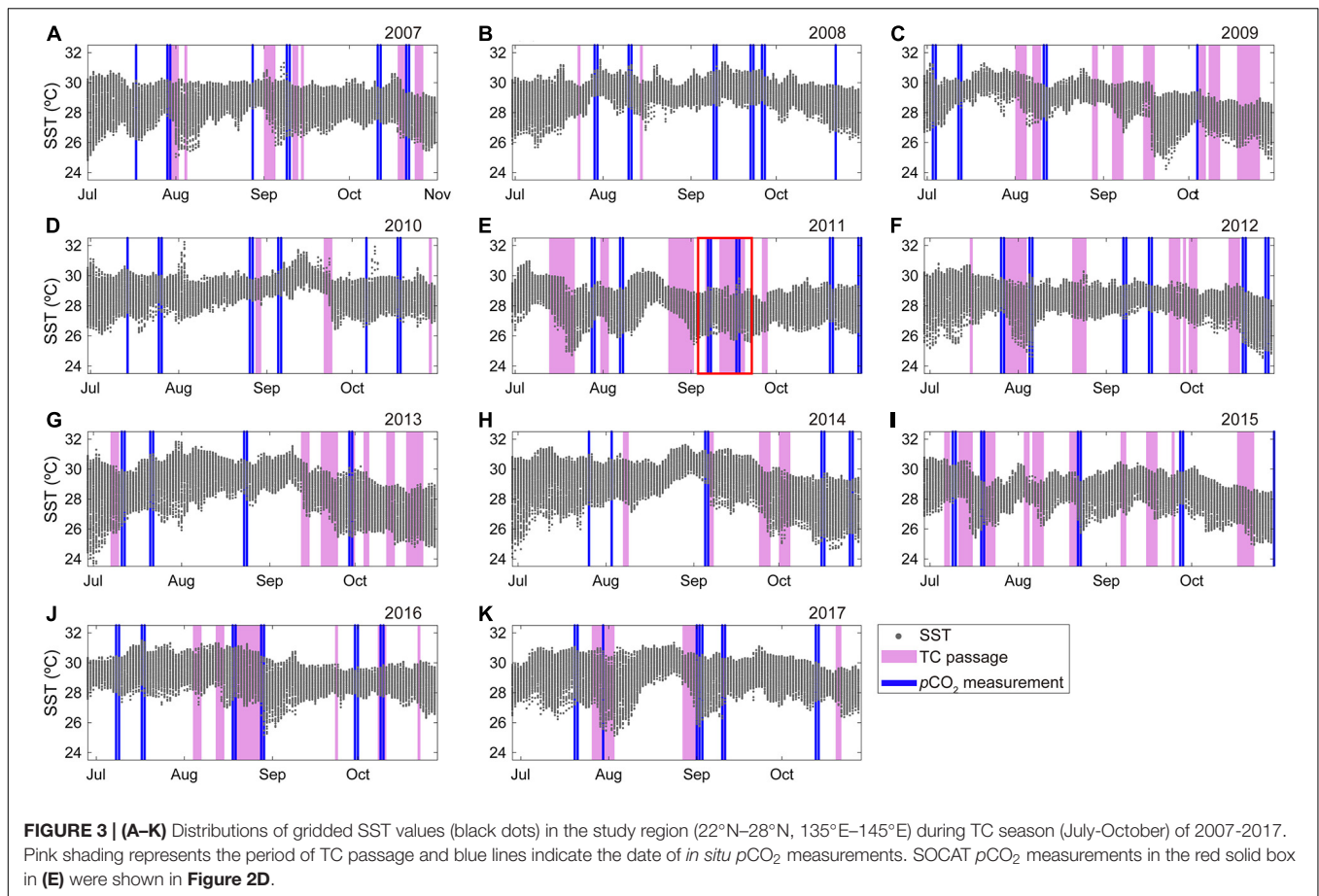
Calculation of Air–Sea CO_2 Flux

The air–sea CO_2 flux (F) was calculated using the following equation:

$$F = k \times \alpha \times \Delta p\text{CO}_2 \quad (4)$$

where k is the CO_2 gas transfer velocity, α is the solubility of CO_2 in seawater (Weiss, 1974), and $\Delta p\text{CO}_2$ is the air–sea $p\text{CO}_2$ difference (atmospheric value minus seawater value). k is calculated using the following equation:

$$k = 0.251 \times (\text{Sc}/660)^{-1/2} \times (U_{10})^2 \quad (5)$$



where Sc is the Schmidt number, U_{10} is the wind speed (m s^{-1}) at 10 m height, and 0.251 is a scaling factor (Wanninkhof, 2014). The daily air–sea CO_2 fluxes were estimated for the TC season (July–October) according to the following procedures. First, SST and $p\text{CO}_2$ values were averaged in each SOCAT survey. To fill the gap in temporal coverage, the thermodynamic temperature coefficient ($\partial \ln p\text{CO}_2 / \partial \text{SST} = 0.0423 \text{ }^\circ\text{C}^{-1}$) was applied to correct for an SST increase for the warming period. For the cooling period, daily $p\text{CO}_2$ values were predicted from the water-column T– $p\text{CO}_2$ relationship derived from GLODAP v2 data (Olsen et al., 2016) in the upper 60 m, which was performed to reflect the effect of vertical mixing on the SST drop during the cooling period.

RESULTS AND DISCUSSION

Seasonal and Interannual $p\text{CO}_2$ Variations Associated With TC-Driven Vertical Mixing

The time series of surface $p\text{CO}_2$ data in the study area (22°N–28°N, 135°E–145°E) clearly showed a long-term secular increasing trend ($\sim 2.2 \mu\text{atm year}^{-1}$) during 2007–2017 (see Data and Methods section) and high seasonal variation ($\sim 80 \mu\text{atm}$)

(**Figure 1A**). The SST variation of $\sim 6^\circ\text{C}$ and the corresponding thermal effect on $p\text{CO}_2$ were responsible for the seasonal $p\text{CO}_2$ amplitude of $100\text{--}130 \mu\text{atm}$ (**Figure 1B**), which was comparable to that observed at a site (ALOHA station; 22°N and 148°W) with environmental conditions similar to those of the present study area (Sutton et al., 2017). The large thermal effects (elevated and reduced $p\text{CO}_2$ in the warm and cool seasons, respectively) were partly canceled out by the biological drawdown of CO_2 during the transition from spring to autumn and the entrainment of CO_2 -rich water in winter, respectively (**Figure 1B**). The average reduction rate of $p\text{CO}_2^{\text{net}}$ between March and October was $-4.5 \pm 1.0 \mu\text{atm month}^{-1}$, which could be attributed to a C_T decrease due to net community production (NCP) and a partial offset by air–sea CO_2 exchange. The magnitude of $p\text{CO}_2^{\text{net}}$ increase ($\sim 7 \mu\text{atm}$) due to net air-to-sea CO_2 flux obtained from monthly climatology (Landschützer et al., 2020) was close to 20% of the NCP-derived $p\text{CO}_2^{\text{net}}$ decrease during the warming period.

While seasonal variations in surface $p\text{CO}_2$ were largely controlled by seasonal variations in SST, vertical mixing, and biological activities, during the TC months (August–October), TC events cause a seasonal deviation of SST and $p\text{CO}_2$ because TC winds cool the sea surface in warm seasons through Ekman upwelling and vertical turbulent mixing (Price, 1981; D’Asaro et al., 2007; Zhang et al., 2021). For example, after a TC passage in 2011, an SST drop of $>3^\circ\text{C}$ was detected with a significant

decrease in $p\text{CO}_2$ over the area centered at $\sim 140^\circ\text{E}$ (Figure 2C). The effect of TC-driven upwelling on $p\text{CO}_2$ can be assessed using $p\text{CO}_2^{\text{nt}}$ values with the assumption that the TC-driven enhancement of nutrients has a negligible effect (the effect of nutrient upwelling is discussed in the following section). The $p\text{CO}_2^{\text{nt}}$ values along the TC track in 2011 were greater by 20–40 μatm than the monthly climatological $p\text{CO}_2^{\text{nt}}$ value (330–360 μatm ; Fassbender et al., 2017; Figure 2D). We hypothesized that this discrepancy was due to the TC-driven upwelling of CO_2 -rich waters, which is comparable to the seasonal drawdown (~ 32 μatm) of the $p\text{CO}_2^{\text{nt}}$ values resulting from biophysical processes (NCP and net air–sea CO_2 exchange).

To support our hypothesis, we compared the SOCAT $p\text{CO}_2^{\text{nt}}$ and SST during 2007–2017 in the study area, because a decrease in SST can represent the degree of mixing when it is used in conjunction with $p\text{CO}_2^{\text{nt}}$. Additionally, rather than examining the effect of individual TC events, this study focused on the integrated effect of TC events on $p\text{CO}_2$ during the TC period, which was usually between August and October. Although July is affected by TCs, we removed the July $p\text{CO}_2$ data in this analysis because TC occurrence was the least frequent in July. This data removal can minimize a potential bias caused by spatiotemporal mismatches between $p\text{CO}_2$ observations and TC events (this is discussed again at the end of this section). In this regard, the $p\text{CO}_2^{\text{nt}}$ (tcm- $p\text{CO}_2^{\text{nt}}$) was averaged over the TC months (August–October) each year, which ranged from 346 to 359 μatm over 2007–2017 (Figure 4A). Similarly, the mean SST (tcm-SST) and ACE index (tcm-ACE) over the TC months were calculated for every year. The comparisons among these metrics for TC months gave significant linear correlations between the tcm- $p\text{CO}_2^{\text{nt}}$ values and the tcm-ACE ($r = 0.81$, $p < 0.01$), and between the tcm- $p\text{CO}_2^{\text{nt}}$ and the tcm-SST ($r = -0.75$, $p < 0.01$). In other words, the years with enhanced cooling and more frequent and intense TC events (as estimated by the ACE index) had elevated $p\text{CO}_2^{\text{nt}}$ values, suggesting the influence of TC-induced vertical mixing (i.e., SST drop) on the interannual variability of $p\text{CO}_2$. There was a positive correlation between the MLD and ACE index of a given TC month over the study year ($r = 0.48$, 0.47, and 0.82 for August, September, and October, respectively), which implied that TC activities deepened the MLD. The effect of TCs on $p\text{CO}_2^{\text{nt}}$ was further supported by the presence of enhanced wind speed (strongly correlated with the tcm-ACE, $r = 0.88$, $p < 0.01$) during years with low SST (Figure 4B). For example, the largest SST decrease (-2.9°C) and the highest wind speed (~ 8.2 m s^{-1}) during TC months were observed in 2013, when the most intense TC activity was recorded (Figures 4B,D). All variables collectively indicated $p\text{CO}_2$ enhancement caused by deeper mixing associated with TC-driven wind speed increments.

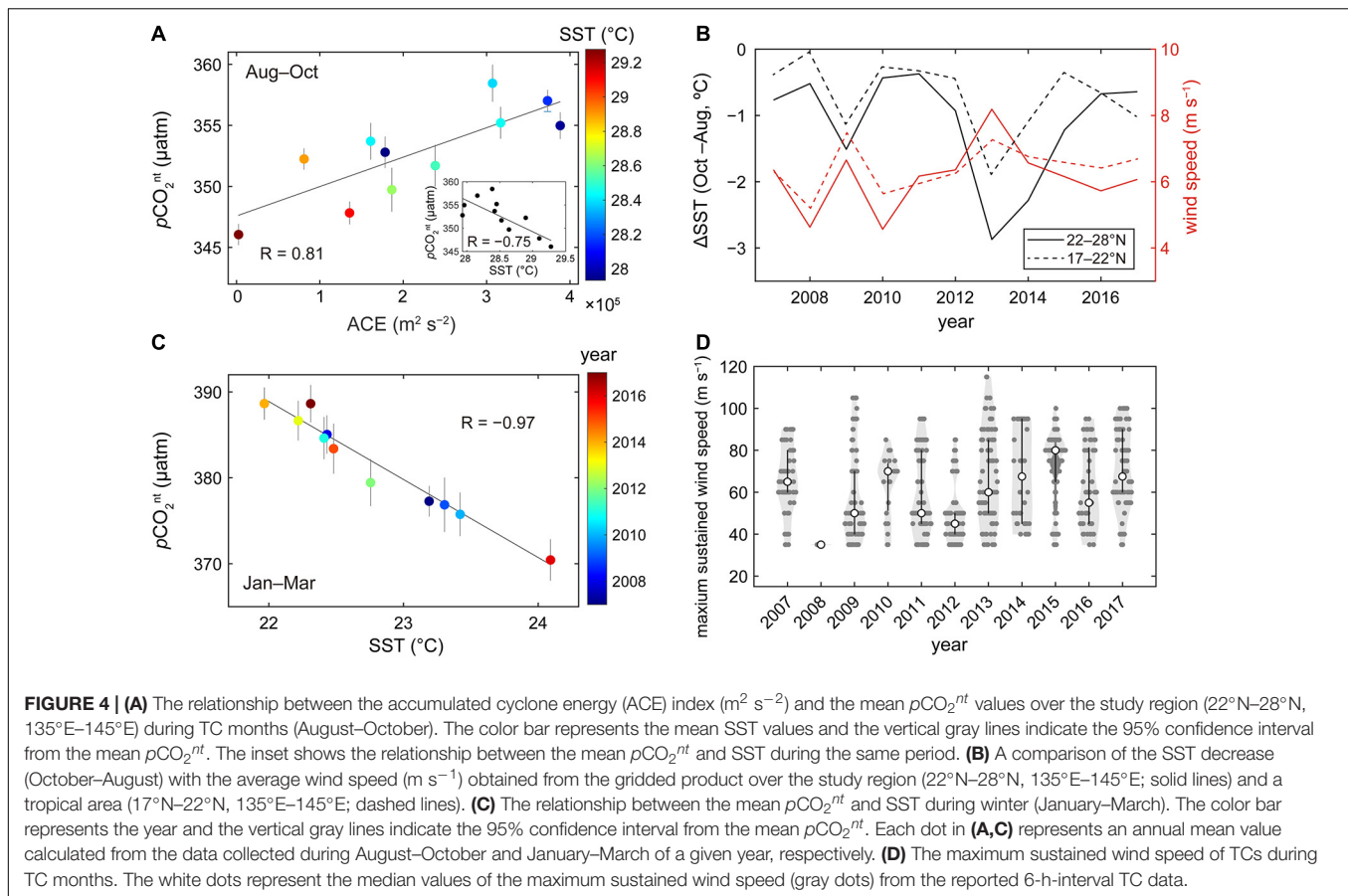
Some SOCAT $p\text{CO}_2$ data measured prior to TC events were included in our analysis because we used all $p\text{CO}_2$ data collected over the TC months (August–October) when calculating the average values. The inclusion of such data that are unaffected by TC events could lead to the underestimation of the magnitude of $p\text{CO}_2$ variability directly caused by TCs. In other words, our results obtained based on SOCAT $p\text{CO}_2$ values may not provide an accurate estimation of the TC effect on $p\text{CO}_2$ during the days of direct TC influences. Instead, the variation in averaged

$p\text{CO}_2$ determined in this study reflects the TC effect on vertical mixing during the period defined as “TC months” (August–October). Another possibility is that an unidentified factor, such as large-scale oceanic and atmospheric variabilities, could favor more frequent TCs and enhanced mixing. In the study region (22°N – 28°N , 135°E – 145°E), however, interannual variations in $p\text{CO}_2^{\text{nt}}$ during TC months were not correlated with the Pacific Meridional Mode or Central Pacific El Niño, which have been reported to be related to basin-wide TC occurrence in the western North Pacific Ocean (Gao et al., 2020).

Because SOCAT SST data (which were collected simultaneously with $p\text{CO}_2$) were used in this analysis, and their spatiotemporal coverage is limited, we compared these SST data with NOAA gridded SST data, which can better represent the mean conditions during the TC months (August–October) and over the study regions. It was found that the seasonal mean values of the SOCAT SST were consistent with those of the NOAA gridded SST, giving a significant correlation ($r = 0.93$, $p < 0.01$). Because the NOAA dataset is based mainly on satellite observations covering large areas, the overall consistency between the two SST datasets indicates that the effect of TC events was usually extensive over the study area, and thus the effects of TCs on SST could be included in the SOCAT SST. Additionally, the consistency between the NOAA and SOCAT SST data implies that the SOCAT $p\text{CO}_2$ data adequately reflect the general conditions over the study area during TC months.

Influences of Other Factors on $p\text{CO}_2^{\text{nt}}$ Variations

The TC-driven upwelling of subsurface waters with elevated levels of CO_2 and nutrients can have two competing effects on $p\text{CO}_2^{\text{nt}}$. However, the significant positive correlation between the interannual variations in $p\text{CO}_2^{\text{nt}}$ and ACE values (Figure 4A) indicates that the interannual variations in $p\text{CO}_2^{\text{nt}}$ were not mainly caused by the stimulation of phytoplankton photosynthesis in response to new nutrients being supplied during TC events. If the opposite were true (the CO_2 decrease due to post-TC blooming is greater than the CO_2 increase resulting from upwelling), there would be an inverse correlation between $p\text{CO}_2^{\text{nt}}$ and ACE values. The ratio of C_T and NO_3^- in the upwelled subsurface water would be responsible for the greater effect of CO_2 upwelling on the $p\text{CO}_2^{\text{nt}}$ elevation. It was found that, in the study region, the amount of newly supplied nutrients was not sufficient to remove the excess C_T that upwelled simultaneously, because the ratio of vertical gradients between C_T and NO_3^- , which were estimated from the extracted GLODAP v2 data during the TC months (August–October), was ~ 13.7 in the subsurface layer (60–200 m). A C:N ratio greater than the Redfield ratio (i.e., ~ 7) is consistent with the reported C:N ratio (14.3) for vertical flux in the North Pacific subtropical gyre (Letscher et al., 2016). The greater effect of upwelled CO_2 relative to nutrient supply is also supported by the winter data. During January–March, $\sim 94\%$ of the total variance in $p\text{CO}_2^{\text{nt}}$ in our study area was explained by SST (Figure 4C; $r = -0.97$, $p < 0.0001$). Because the thermal effect was removed in $p\text{CO}_2^{\text{nt}}$, the negative correlation between

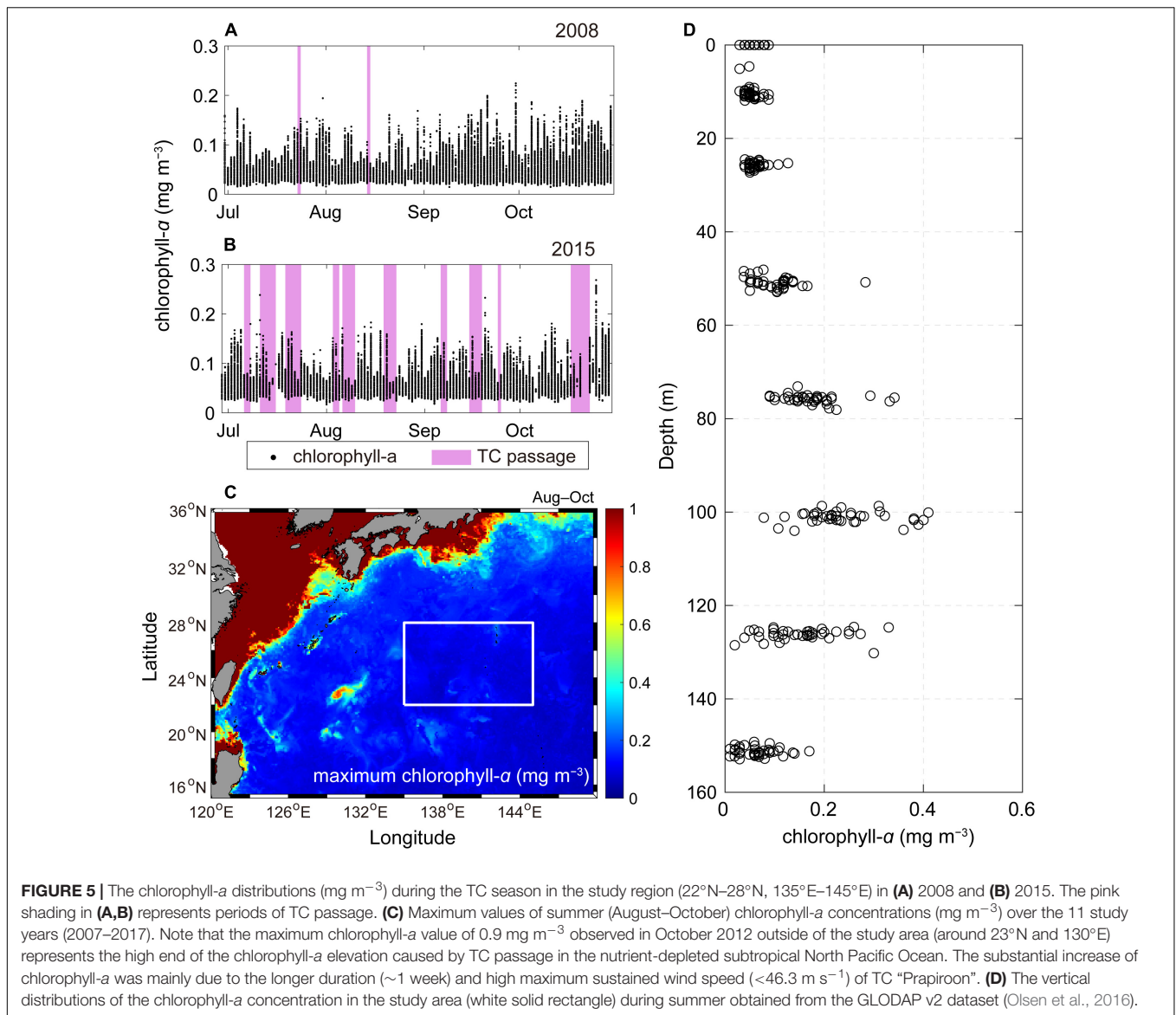


$p\text{CO}_2^{nt}$ and SST means that SST represents a magnitude of vertical winter mixing. During the winter, the phytoplankton production in most of the study area is at least partially limited by NO_3^- concentration ($<0.3 \mu\text{mol kg}^{-1}$), except for the northern boundary area ($>27^\circ\text{N}$) which has a slightly higher concentration ($<1.2 \mu\text{mol kg}^{-1}$).

Subtle changes in chlorophyll-*a* after TC passage indicate a limited contribution of TCs to biological carbon fixation. Surface chlorophyll-*a* values over the TC season (July–October) were not significantly different in 2008 and 2015 despite the significantly different numbers of TCs in these 2 years (Figures 5A,B). Additionally, the maximum chlorophyll-*a* concentration ($<0.3 \text{mg m}^{-3}$) during the TC season (July–October) in 2007–2017 was lower than the difference in chlorophyll-*a* ($\sim 0.4 \text{mg m}^{-3}$) found between the surface and subsurface chlorophyll-*a* maximum layer (SCM) (Figures 5C,D). During the TC season (July–October), the SCM layer ($\sim 100 \text{m}$) was deeper than the maximum MLD ($\sim 80 \text{m}$) derived from Argo temperature profiles (Holte et al., 2017). Thus, it is possible that a slight increase in the surface chlorophyll-*a* after TC passage was not due to enhanced biological activities but instead was the result of mixing with subsurface chlorophyll-*a* because NO_3^- is depleted ($<0.1 \mu\text{mol kg}^{-1}$) in the upper layer ($<80 \text{m}$) during summer. Chai et al. (2021) also observed no increase in the vertically integrated chlorophyll-*a* concentration after TC

passage. However, this conclusion may not be valid in other regions. For example, unlike our study area (a subtropical area with a relatively deep nutricline), the East and South China seas showed enhancements in the chlorophyll-*a* concentration of approximately five times after TC passage (Ye et al., 2013; Wu et al., 2020). This difference may be due to regional variations of the vertical chlorophyll-*a* and nutrient profiles, and especially due to the shallower nutricline of the shelf regions (the East and South China seas), where NO_3^- concentration is one order of magnitude greater than in our study region at 50 m depth.

In a tropical area (17°N – 22°N , 135°E – 145°E) south of our study area, an insignificant relationship was observed between $\text{tcm-}p\text{CO}_2^{nt}$ and tcm-ACE . Over the study period (2007–2017), the NOAA dataset showed that a seasonal SST decrease from August to October ($\Delta\text{SST}_{\text{AUG-OCT}}$) in the tropical area was less than that in our study region despite similar wind speeds in the two regions (6.1 and 6.4m s^{-1} in our study region and the tropical region, respectively) (Figure 4B). For example, in 2013, the $\Delta\text{SST}_{\text{AUG-OCT}}$ was -2.9 and -1.9°C in our study area and the tropical region, respectively. The $p\text{CO}_2^{nt}$ changes in 2013 associated with $\Delta\text{SST}_{\text{AUG-OCT}}$ values could be predicted using the water-column T – $p\text{CO}_2^{nt}$ relationship derived from GLODAP v2 data (Olsen et al., 2016) in the upper 60 m, which were 23 and 15 μatm in the study area and the tropical region, respectively. Smaller variations in SST and $p\text{CO}_2^{nt}$ under similar



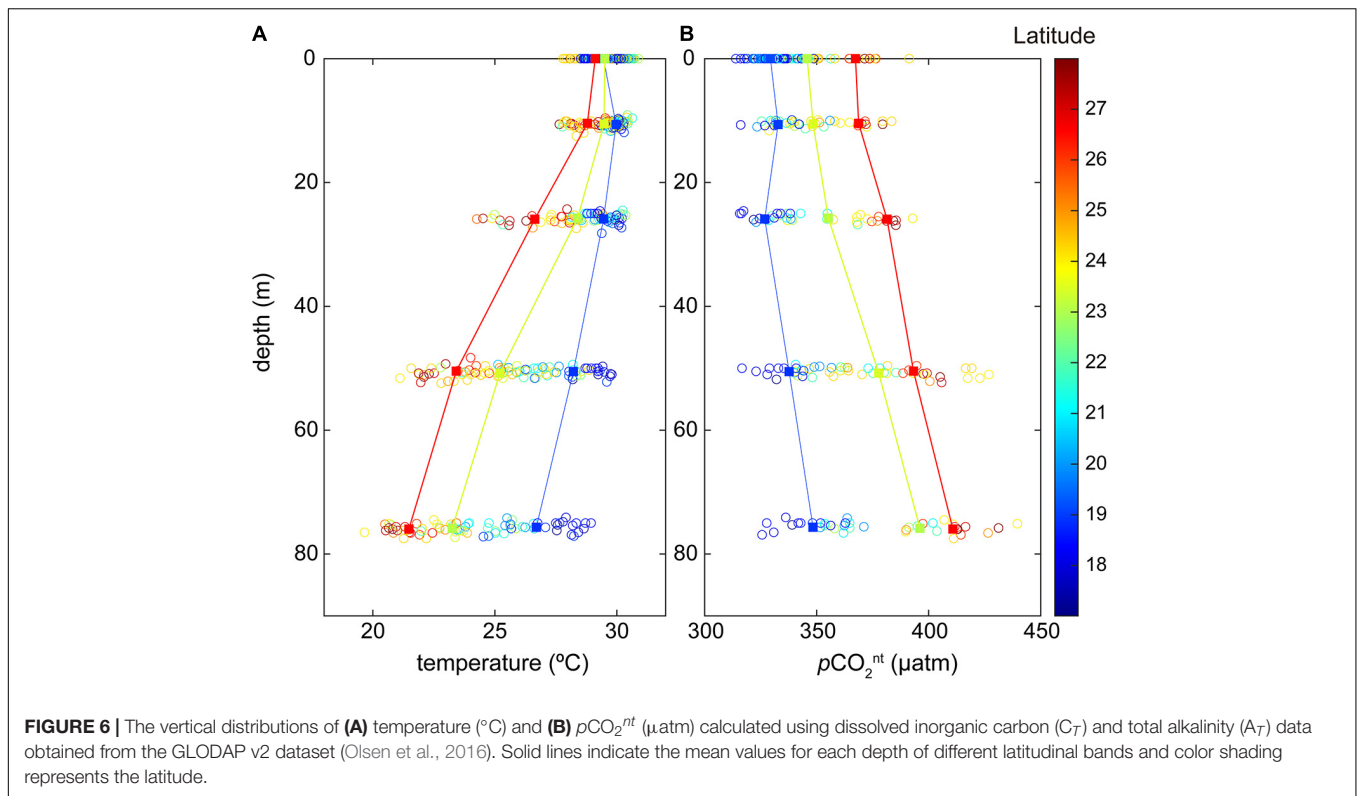
wind forcing (i.e., vertical mixing) could be attributed to the reduced effects of vertical mixing caused by the fact that, in the tropical region, the MLDs were 30–50% deeper (Figure 2A) and the vertical gradients of temperature and $p\text{CO}_2^{nt}$ were less steep (Figure 6), which suggests regionally varying responses to TCs in the North Pacific Ocean.

Salinity variations are usually associated with variations in A_T and C_T . Thus, the mixing of two water masses (e.g., vertical mixing) with different $A_T:C_T$ ratios can significantly modify $p\text{CO}_2^{nt}$ values, which could explain a part of TC-induced changes in $p\text{CO}_2$. Additionally, changes in A_T and C_T associated with precipitation and evaporation (i.e., water balance) within a given water mass alter $p\text{CO}_2$ to a similar magnitude but in an opposite direction (Takahashi et al., 1993). Salinity is also related to the solubility of CO_2 and the dissociation constants of seawater carbonate species, giving the relationship of $(\partial \ln p\text{CO}_2 / \partial \ln \text{salinity}) = 0.93$ for warm waters

(Takahashi et al., 1993). Although it was necessary to correct for the effects of salinity related to water balance on $p\text{CO}_2$, it was not possible to separate salinity variations related to mixing and water balance. Furthermore, the observed salinity variation was not significantly correlated with precipitation ($r < 0.1$; not shown). However, there was a significant correlation between SST and salinity ($r = 0.75$, $p < 0.01$) if removing the outlier in 2016 (not shown), indicating that salinity variations were mainly a consequence of TC-induced mixing in the study area. Thus, the $p\text{CO}_2$ values were not normalized to a constant salinity.

Effects of TC Events on Air–Sea CO_2 Flux

The seasonal $p\text{CO}_2$ evolution modulated by background conditions (e.g., SST, NCP, air–sea CO_2 exchange) and episodic events (e.g., TC) has important implications for the magnitude and direction of air–sea CO_2 flux during and after TC passage.



In the tropical area (17°N – 22°N , 135°E – 145°E), the measured $p\text{CO}_2$ values were lower than the atmospheric $p\text{CO}_2$ during the TC season (July–October). Thus, TC-induced high wind during TC passage and cooling-induced $p\text{CO}_2$ drawdown after TC passage could result in enhanced CO_2 influx from the atmosphere to the ocean. In our study region, the seawater $p\text{CO}_2$ values in July were mostly higher than atmospheric CO_2 , whereas the situation was usually reversed in October (seawater $p\text{CO}_2 <$ atmospheric $p\text{CO}_2$). However, TC events could break this typical $p\text{CO}_2$ trend considerably, leading to a wide range of CO_2 fluxes (from -1.2 to 1.8 g C m^{-2} during July–October) during the study period (2007–2017). It should be noted that these air–sea CO_2 flux estimates have a large uncertainty associated with the assumptions that were made to reconstruct the daily $p\text{CO}_2$ values in the TC season (see Data and Methods section). In an earlier part of the TC season (July–August; a warming period), a substantial TC-driven cooling shifted the study area from a CO_2 source to a CO_2 sink. Although negative $\Delta p\text{CO}_2$ values ($\sim 20 \mu\text{atm}$ higher than atmospheric $p\text{CO}_2$) were expected in July–August due to the high SST ($> 29.5^{\circ}\text{C}$), TC-induced cooling to $\sim 28^{\circ}\text{C}$ in July–September 2011 changed the $\Delta p\text{CO}_2$ value to positive ($\sim 6 \mu\text{atm}$ lower than atmospheric $p\text{CO}_2$). As a result, the TC-driven cooling in 2011 led to the largest oceanic CO_2 uptake ($\sim 1.8 \text{ g C m}^{-2}$) over the July–October period among study years. While the study region was a sink or nearly neutral for atmospheric CO_2 ($0.7 \pm 0.8 \text{ g C m}^{-2} \text{ 4-month}^{-1}$) due to relatively frequent TCs during July–August in 2007, 2010, 2011, and 2015, the study region acted as a CO_2 source ($-0.7 \pm 0.3 \text{ g C m}^{-2} \text{ 4-month}^{-1}$) in the remaining 7 years of the study period. In the

western North Pacific Ocean, a comparable number ($n = 9$ – 10) of TCs was normally generated in the warming (July–August) and cooling (September–October) periods, during which TC-driven outgassing and influx of CO_2 are expected, respectively. However, the uneven occurrence of TCs was also observed in 2018, when 14 and five TC events were generated during July–August and September–October, respectively. These abnormal cases, which are associated with positive phases of the Pacific Meridional Mode and Central Pacific El Niño (Gao et al., 2020), may amplify the interannual variability in the summertime $p\text{CO}_2$ and air–sea CO_2 flux.

Another mixing-related factor that may affect $p\text{CO}_2$ variability is the recovery of the TC-induced SST drop with time. It has been reported that surface heat fluxes could restore the SST to its pre-TC value in ~ 40 days following TC passage (Lévy et al., 2012; Vincent et al., 2012). Thus, TC-induced alternation in the system can carry over to the subsequent month or season. For example, in the study area, the $p\text{CO}_2$ at the mean summer temperature of 29°C is $\sim 401 \mu\text{atm}$, which could be decreased to $373 \mu\text{atm}$ after TC passage with an SST drop of 3°C (arbitrarily chosen value from the TC-driven SST variations shown in Figure 3) and the water-column T – $p\text{CO}_2^{\text{nt}}$ relationship derived from GLODAP v2 data (Olsen et al., 2016) in the upper 60 m of the study region. Warming back to the original temperature or greater during the warming period (normally July–August) raises the surface $p\text{CO}_2$ to $> 423 \mu\text{atm}$ based on the relationship $\partial \ln p\text{CO}_2 / \partial \text{SST} = 0.0423^{\circ}\text{C}^{-1}$; this shifts the given water mass from a CO_2 sink to a CO_2 source, thus canceling out at least part of the TC-driven

enhancement in the CO_2 uptake. In this case, if it is assumed that temperature recovery occurs during a given month, TC-induced mixing can increase the sea-surface $p\text{CO}_2$ in the following month by $\sim 22 \mu\text{atm}$. However, TC-induced cooling could not be recovered if the TC event occurred during the cooling period, meaning that the given water mass would remain as a CO_2 sink. As indicated, because of the variable magnitude and duration of the thermal and non-thermal impact of TC events on $p\text{CO}_2$, the application of the general temperature correlation ($\partial \ln p\text{CO}_2 / \partial \text{SST} = 0.0423^\circ\text{C}^{-1}$) or local empirical $p\text{CO}_2$ -SST relationship may produce biased estimates of the year-to-year variability of $p\text{CO}_2$ and CO_2 flux, particularly in summer.

CONCLUSION AND IMPLICATION

The effect of TC-driven mixing on sea-surface $p\text{CO}_2$ was evaluated over the 2007–2017 period based on high-quality ship-based observational data. The ACE index, a proxy for the overall intensity of TC events, was linearly correlated with $p\text{CO}_2^{nt}$, which was used to represent temperature-independent $p\text{CO}_2$, suggesting the possible TC-induced enhancement of the upwelling of deep waters with greater C_T and $p\text{CO}_2^{nt}$ in the study area. In this regard, interannual variations in TC activities appeared to have contributed to a $p\text{CO}_2$ variability as large as $\sim 13 \mu\text{atm}$ of $\text{tcm-}p\text{CO}_2^{nt}$ over the 11 study years. Because we did not focus on all TC events case-by-case and used averaged values over the given TC months (August–October), our findings do not represent the immediate $p\text{CO}_2$ response following a TC event. Instead, our results suggest that $p\text{CO}_2^{nt}$ is elevated with reduced SST during years with greater TC influence. Therefore, we conclude that the effects of TC-driven mixing on SST and $p\text{CO}_2$ need to be more thoroughly investigated to accurately estimate the natural variability of summer $p\text{CO}_2$ and CO_2 flux from long-term $p\text{CO}_2$ observations.

The impact of TC-induced mixing on surface $p\text{CO}_2^{nt}$ can be significant throughout the westmost side of the western subtropical Pacific Ocean including the East Asian marginal seas, which encounter a considerable number of intense TCs. However, it was not possible to reveal the basin-wide effects of TC activity on the sea-surface $p\text{CO}_2$ and air–sea CO_2 flux because of sparse coverage of $p\text{CO}_2$ data and different regional responses that are dependent on pre-existing oceanic conditions. Furthermore, it has been predicted that climate warming will decrease the global frequency of TCs but enhance their overall intensity (Knutson et al., 2010; Christensen et al., 2013). Because the direct effect of climate warming (thermal effects) on $p\text{CO}_2$ and indirect effects such as enhanced stratification and increased TC activity are expected to further complicate the spatiotemporal variabilities in summertime $p\text{CO}_2$ in the future, *in situ* $p\text{CO}_2$ observations need to be extended to the entire northwestern Pacific Ocean.

DATA AVAILABILITY STATEMENT

Publicly available datasets were analyzed in this study. This data can be found here and Data and Methods section: Surface Ocean CO_2 Atlas (<http://www.socat.info/>); Regional Specialized Meteorological Center of the Japan Meteorological Agency (https://www.jma.go.jp/jma/jma-eng/jma-center/rsmc-hp-pub-eg/RSMC_HP.htm); the climatological MLD database derived from Argo profiles (<http://www.argo.ucsd.edu>); Global Ocean Data Analysis Project version 2 (<https://www.nodc.noaa.gov/ocads/oceans/GLODAPv2/>); ocean color webpage operated by the National Aeronautics and Space Administration (<https://oceancolor.gsfc.nasa.gov/>); $\Delta p\text{CO}_2$ (atmospheric $p\text{CO}_2$ minus seawater $p\text{CO}_2$) climatology data (https://www.ncei.noaa.gov/access/ocean-carbon-data-system/oceans/SPCO2_1982_present_ETH_SOM_FFN.html); National Oceanic and Atmospheric Administration high-resolution SST data (<https://www.esrl.noaa.gov/psd/>); the gridded daily 10-m wind speed data (<https://psl.noaa.gov/data/gridded/data.ncep.reanalysis.html>); monthly precipitation data (<https://psl.noaa.gov/data/gridded/data.cmap.html>).

AUTHOR CONTRIBUTIONS

YK analyzed the data and wrote the original draft. DK designed the study. G-HP and T-WK contributed to the manuscript. All authors approved the submitted version.

FUNDING

This work was supported by the Basic Science Research Program of the National Research Foundation of Korea (NRF-2019R1A2C2089994), a project (PE99912) of the Korea Institute of Ocean Science and Technology, a Korea University Grant, and a project (study on air–sea interaction and process of rapidly intensifying typhoons in the Northwestern Pacific) funded by the Ministry of Oceans and Fisheries, South Korea.

ACKNOWLEDGMENTS

The SOCAT is an international effort, endorsed by the International Ocean Carbon Coordination Project (IOCCP), the Surface Ocean Lower Atmosphere Study (SOLAS), and the Integrated Marine Biosphere Research (IMBeR) program, to deliver a uniformly quality-controlled surface ocean CO_2 database. The authors appreciate all researchers and funding agencies, especially Yukihiro Nojiri who provided almost all $p\text{CO}_2$ data used in this study. This work was not possible without his valuable contribution to the collection of a high-quality $p\text{CO}_2$ data in the northwestern Pacific Ocean.

REFERENCES

- Bakker, D. C. E., Pfeil, B., Landa, C. S., Metzl, N., O'Brien, K. M., Olsen, A., et al. (2016). A multi-decade record of high-quality fCO₂ data in version 3 of the Surface Ocean CO₂ Atlas (SOCAT). *Earth Syst. Sci. Data* 8, 383–413. doi: 10.5194/essd-8-383-2016
- Bates, N. R., Knap, A. H., and Michaels, A. F. (1998). Contribution of hurricanes to local and global estimates of air-sea exchange of CO₂. *Nature* 395, 58–61. doi: 10.1038/25703
- Bell, G. D., Halpert, M. S., Schnell, R. C., Higgins, R. W., Lawrimore, J., Kousky, V. E., et al. (2000). Climate assessment for 1999. *Bull. Amer. Meteor. Soc.* 81, S1–S50.
- Bond, N. A., Cronin, M. F., Sabine, C., Kawai, Y., Ichikawa, H., Freitag, P., et al. (2011). Upper ocean response to typhoon choi-wan as measured by the kuroshio extension observatory mooring. *J. Geophys. Res. Oceans* 116:C02031. doi: 10.1029/2010jc006548
- Chai, F., Wang, Y., Xing, X., Yan, Y., Xue, H., Wells, M., et al. (2021). A limited effect of sub-tropical typhoons on phytoplankton dynamics. *Biogeosciences* 18, 849–859. doi: 10.5194/bg-18-849-2021
- Chen, F., Cai, W.-J., Benitez-Nelson, C., and Wang, Y. (2007). Sea surface pCO₂-SST relationships across a cold-core cyclonic eddy: implications for understanding regional variability and air-sea gas exchange. *Geophys. Res. Lett.* 34:L10603. doi: 10.1029/2006gl028058
- Cheng, L., Zhu, J., and Srivier, R. L. (2015). Global representation of tropical cyclone-induced short-term ocean thermal changes using Argo data. *Ocean Sci.* 11, 719–741. doi: 10.5194/os-11-719-2015
- Christensen, J. H., Kanikicharla, K. K., Aldrian, E., An, S. I., Cavalcanti, I. F. A., de Castro, M., et al. (2013). *Climate Phenomena and Their Relevance for Future Regional Climate Change. In Climate Change 2013 The Physical Science Basis: Working Group I Contribution to the Fifth Assessment Report of the Intergovernmental Panel on Climate Change.* Cambridge: Cambridge University Press, 1217–1308. doi: 10.1017/CBO9781107415324.028
- D'Asaro, E. A., Sanford, T. B., Niiler, P. P., and Terrill, E. J. (2007). Cold wake of hurricane Frances. *Geophys. Res. Lett.* 34:L15609. doi: 10.1029/2007gl030160
- Fassbender, A. J., Rodgers, K. B., Palevsky, H. I., and Sabine, C. L. (2018). Seasonal asymmetry in the evolution of surface ocean pCO₂ and pH thermodynamic drivers and the influence on sea-air CO₂ flux. *Global Biogeochem. Cycles* 32, 1476–1497. doi: 10.1029/2017gb005855
- Fassbender, A. J., Sabine, C. L., and Palevsky, H. I. (2017). Nonuniform ocean acidification and attenuation of the ocean carbon sink. *Geophys. Res. Lett.* 44, 8404–8413. doi: 10.1002/2017gl074389
- Gao, S., Zhu, L., Zhang, W., and Shen, X. (2020). Western north pacific tropical cyclone activity in 2018: a season of extremes. *Sci. Rep.* 10:5610. doi: 10.1038/s41598-020-62632-5
- Holte, J., Talley, L. D., Gilson, J., and Roemmich, D. (2017). An Argo mixed layer climatology and database. *Geophys. Res. Lett.* 44, 5618–5626. doi: 10.1002/2017gl073426
- Huang, P., and Imberger, J. (2010). Variation of pCO₂ in ocean surface water in response to the passage of a hurricane. *J. Geophys. Res.* 115:C10024. doi: 10.1029/2010JC006185
- Kalnay, E., Kanamitsu, M., Kistler, R., Collins, W., Deaven, D., Gandin, L., et al. (1996). The NCEP/NCAR 40-year reanalysis project. *B. Am. Meteorol. Soc.* 77, 437–472. doi: 10.1175/1520-04771996077<0437:Tnyrp>2.0.Co;2
- Knutson, T. R., McBride, J. L., Chan, J., Emanuel, K., Holland, G., Landsea, C., et al. (2010). Tropical cyclones and climate change. *Nat. Geosci.* 3, 157–163. doi: 10.1038/ngeo779
- Landschützer, P., Gruber, N., and Bakker, D. C. E. (2016). Decadal variations and trends of the global ocean carbon sink. *Global Biogeochem. Cycles* 30, 1396–1417. doi: 10.1002/2015gb005359
- Landschützer, P., Gruber, N., Bakker, D. C. E., Stemmler, I., and Six, K. D. (2018). Strengthening seasonal marine CO₂ variations due to increasing atmospheric CO₂. *Nat. Clim. Change* 8, 146–150. doi: 10.1038/s41558-017-0057-x
- Landschützer, P., Laruelle, G. G., Roobaert, A., and Regnier, P. (2020). A uniform pCO₂ climatology combining open and coastal oceans. *Earth Syst. Sci. Data* 12, 2537–2553. doi: 10.5194/essd-12-2537-2020
- Lenton, A., Metzl, N., Takahashi, T., Kuchinke, M., Matear, R. J., Roy, T., et al. (2012). The observed evolution of oceanic pCO₂ and its drivers over the last two decades. *Global Biogeochem. Cycles* 26:GB2021. doi: 10.1029/2011gb004095
- Letscher, R. T., Primeau, F., and Moore, J. K. (2016). Nutrient budgets in the subtropical ocean gyres dominated by lateral transport. *Nat. Geosci.* 9, 815–819. doi: 10.1038/ngeo2812
- Lévy, M., Lengaigne, M., Bopp, L., Vincent, E. M., Madec, G., Ethé, C., et al. (2012). Contribution of tropical cyclones to the air-sea CO₂ flux: a global view. *Global Biogeochem. Cycles* 26:GB2001. doi: 10.1029/2011gb004145
- Lin, I.-I. (2012). Typhoon-induced phytoplankton blooms and primary productivity increase in the western North Pacific subtropical ocean. *J. Geophys. Res. Oceans* 117:C03039. doi: 10.1029/2011jc007626
- Lueker, T. J., Dickson, A. G., and Keeling, C. D. (2000). Ocean pCO₂ calculated from dissolved inorganic carbon, alkalinity, and equations for K₁ and K₂: validation based on laboratory measurements of CO₂ in gas and seawater at equilibrium. *Mar. Chem.* 70, 105–119. doi: 10.1016/S0304-4203(00)00022-0
- Mahadevan, A., Tagliabue, A., Bopp, L., Lenton, A., Mémerly, L., and Lévy, M. (2011). Impact of episodic vertical fluxes on sea surface pCO₂. *Philos. T. R. Soc. A.* 369, 2009–2025. doi: 10.1098/rsta.2010.0340
- Nemoto, K., Midorikawa, T., Wada, A., Ogawa, K., Takatani, S., Kimoto, H., et al. (2009). Continuous observations of atmospheric and oceanic CO₂ using a moored buoy in the East China Sea: variations during the passage of typhoons. *Deep Sea Res. Pt. II* 56, 542–553. doi: 10.1016/j.dsr2.2008.12.015
- Olsen, A., Key, R. M., van Heuven, S., Lauvset, S. K., Velo, A., Lin, X., et al. (2016). The Global Ocean Data Analysis Project version 2 (GLODAPv2)—an internally consistent data product for the world ocean. *Earth Syst. Sci. Data* 8, 297–323. doi: 10.5194/essd-8-297-2016
- Ono, H., Kosugi, N., Toyama, K., Tsujino, H., Kojima, A., Enyo, K., et al. (2019). Acceleration of ocean acidification in the Western North Pacific. *Geophys. Res. Lett.* 46, 13161–13169. doi: 10.1029/2019gl085121
- Price, J. F. (1981). Upper ocean response to a hurricane. *J. Phys. Oceanogr.* 11, 153–175. doi: 10.1175/1520-04851981011<0153:Uortah>2.0.Co;2
- Sutton, A. J., Wanninkhof, R., Sabine, C. L., Feely, R. A., Cronin, M. F., and Weller, R. A. (2017). Variability and trends in surface seawater pCO₂ and CO₂ flux in the Pacific Ocean. *Geophys. Res. Lett.* 44, 5627–5636. doi: 10.1002/2017gl073814
- Takahashi, T., Olafsson, J., Goddard, J. G., Chipman, D. W., and Sutherland, S. C. (1993). Seasonal variation of CO₂ and nutrients in the high-latitude surface oceans: a comparative study. *Global Biogeochem. Cycles* 7, 843–878. doi: 10.1029/93gb02263
- Takahashi, T., Sutherland, S. C., Feely, R. A., and Wanninkhof, R. (2006). Decadal change of the surface water pCO₂ in the North Pacific: a synthesis of 35 years of observations. *J. Geophys. Res. Oceans* 111:C07S05. doi: 10.1029/2005jc003074
- Takahashi, T., Sutherland, S. C., and Kozyr, A. (2019). *Global Ocean Surface Water Partial Pressure of CO₂ Database: Measurements Performed During 1957–2018 (LDEO Database Version 2018) (NCEI Accession 0160492). Version 7.7.* NOAA National Centers for Environmental Information. Dataset. Asheville NC: NOAA National Centers for Environmental Information, doi: 10.3334/CDIAC/OTG.NDP088(V2015)
- Takahashi, T., Sutherland, S. C., Sweeney, C., Poisson, A., Metzl, N., Tilbrook, B., et al. (2002). Global sea-air CO₂ flux based on climatological surface ocean pCO₂, and seasonal biological and temperature effects. *Deep Sea Res. Pt. II* 49, 1601–1622. doi: 10.1016/S0967-0645(02)00003-6
- Takahashi, T., Sutherland, S. C., Wanninkhof, R., Sweeney, C., Feely, R. A., Chipman, D. W., et al. (2009). Climatological mean and decadal change in surface ocean pCO₂, and net sea-air CO₂ flux over the global oceans. *Deep Sea Res. Pt. II* 56, 554–577. doi: 10.1016/j.dsr2.2008.12.009
- Vincent, E. M., Lengaigne, M., Madec, G., Vialard, J., Samson, G., Jourdain, N. C., et al. (2012). Processes setting the characteristics of sea surface cooling induced by tropical cyclones. *J. Geophys. Res. Oceans* 117:C02020. doi: 10.1029/2011JC007396
- Wada, A., Cronin, M. F., Sutton, A. J., Kawai, Y., and Ishii, M. (2013). Numerical simulations of oceanic pCO₂ variations and interactions between Typhoon Choi-wan (0914) and the ocean. *J. Geophys. Res. Oceans* 118, 2667–2684. doi: 10.1002/jgrc.20203
- Wada, A., Uehara, T., and Ishizaki, S. (2014). Typhoon-induced sea surface cooling during the 2011 and 2012 typhoon seasons: observational evidence and numerical investigations of the sea surface cooling effect using typhoon simulations. *Prog. Earth Planet. Sci.* 1:11. doi: 10.1186/2197-4284-1-11
- Wanninkhof, R. (2014). Relationship between wind speed and gas exchange over the ocean revisited. *Limnol. Oceanogr. Meth.* 12, 351–362. doi: 10.4319/lom.2014.12.351

- Wanninkhof, R., Olsen, A., and Triñanes, J. (2007). Air–sea CO₂ fluxes in the Caribbean Sea from 2002–2004. *J. Mar. Syst.* 66, 272–284. doi: 10.1016/j.jmarsys.2005.11.014
- Wanninkhof, R., Park, G. H., Takahashi, T., Sweeney, C., Feely, R., Nojiri, Y., et al. (2013). Global ocean carbon uptake: magnitude, variability and trends. *Biogeosciences* 10, 1983–2000. doi: 10.5194/bg-10-1983-2013
- Weiss, R. F. (1974). Carbon dioxide in water and seawater: the solubility of a non-ideal gas. *Mar. Chem.* 2, 203–215. doi: 10.1016/0304-4203(74)90015-2
- Wu, Y., Dai, M., Guo, X., Chen, J., Xu, Y., Dong, X., et al. (2020). High-frequency time-series autonomous observations of sea surface pCO₂ and pH. *Limnol. Oceanogr.* 66, 588–606. doi: 10.1002/lno.11625
- Ye, H., Morozov, E., Tang, D., Wang, S., Liu, Y., Li, Y., et al. (2020). Variation of pCO₂ concentrations induced by tropical cyclones “Wind-Pump” in the middle-latitude surface oceans: a comparative study. *PLoS One* 15:e0226189. doi: 10.1371/journal.pone.0226189
- Ye, H., Sheng, J., Tang, D., Siswanto, E., Ali Kalhor, M., and Sui, Y. (2017). Storm-induced changes in pCO₂ at the sea surface over the northern South China Sea during Typhoon Wutip. *J. Geophys. Res. Oceans* 122, 4761–4778. doi: 10.1002/2016jc012643
- Ye, H. J., Sui, Y., Tang, D. L., and Afanasyev, Y. D. (2013). A subsurface chlorophyll a bloom induced by typhoon in the South China Sea. *J. of Mar. Syst.* 128, 138–145. doi: 10.1016/j.jmarsys.2013.04.010
- Zhang, H., He, H., Zhang, W.-Z., and Tian, D. (2021). Upper ocean response to tropical cyclones: a review. *Geosci. Lett.* 8:1. doi: 10.1186/s40562-020-00170-8

Conflict of Interest: The authors declare that the research was conducted in the absence of any commercial or financial relationships that could be construed as a potential conflict of interest.

Copyright © 2021 Ko, Park, Kim and Kim. This is an open-access article distributed under the terms of the Creative Commons Attribution License (CC BY). The use, distribution or reproduction in other forums is permitted, provided the original author(s) and the copyright owner(s) are credited and that the original publication in this journal is cited, in accordance with accepted academic practice. No use, distribution or reproduction is permitted which does not comply with these terms.